Digital access to libraries

"Hepatocellular carcinoma originates from hepatocytes and not from the progenitor/biliary compartment."

Mu, Xueru ; Español-Suñer, Regina ; Mederacke, Ingmar ; Affò, Silvia ; Manco, Rita ; Sempoux, Christine ; Lemaigre, Frédéric ; Adili, Arlind ; Yuan, Detian ; Weber, Achim ; Unger, Kristian ; Heikenwälder, Mathias ; Leclercq, Isabelle ; Schwabe, Robert F

Abstract

In many organs, including the intestine and skin, cancers originate from cells of the stem or progenitor compartment. Despite its nomenclature, the cellular origin of hepatocellular carcinoma (HCC) remains elusive. In contrast to most organs, the liver lacks a defined stem cell population for organ maintenance. Previous studies suggest that both hepatocytes and facultative progenitor cells within the biliary compartment are capable of generating HCC. As HCCs with a progenitor signature carry a worse prognosis, understanding the origin of HCC is of clinical relevance. Here, we used complementary fate-tracing approaches to label the progenitor/biliary compartment and hepatocytes in murine hepatocarcinogenesis. In genotoxic and genetic models, HCCs arose exclusively from hepatocytes but never from the progenitor/biliary compartment. Cytokeratin 19-, A6- and α-fetoprotein-positive cells within tumors were hepatocyte derived. In summary, hepatocytes represent the cell of origin for HCC i...

Document type : *Article de périodique (Journal article)*

Référence bibliographique

Hepatocellular carcinoma originates from hepatocytes and not from progenitor cells

Xueru Mu[1,2]†, Regina Espanol-Suner[3]†, Ingmar Mederacke[1], Silvia Affo[1], Rita Manco[3], Christine Sempoux[4], Frederic Lemaigre[5], Arlind Adili[6], Detian Yuan[6], Achim Weber[7], Kristian Unger[8], Mathias Heikenwälder[6], Isabelle Leclercq[3]* and Robert F. Schwabe[1]*

[1]Department of Medicine, Columbia University, New York, NY 10032, USA

[2]Institute of Oncology, Provincial Hospital Affiliated to Shandong University, Shandong University, Jinan, P. R. China

[3]Laboratory of Hepato-Gastroenterology, Institut de Recherche Expérimentale et Clinique, Université catholique de Louvain, 1200 Brussels, Belgium

[4]Department of Pathology, St Luc University Hospital and Université catholique de Louvain, 1200 Brussels, Belgium

[5]Liver and Pancreas Development Unit, de Duve Institute, Université catholique de Louvain, Brussels, Belgium.

[6] Institute of Virology, Technische Universität München/Helmholtz Zentrum München, Munich, D-81675 Germany

[7]Institute of Surgical Pathology, University Hospital Zurich, Zurich, CH-8091 Switzerland

[8]Research Unit of Radiation Cytogenetics, Helmholtz Zentrum München, German Research Center for Environmental Health, Neuherberg, D-85764 Germany

Correspondence to: Robert F. Schwabe, rfs2102@cumc.columbia.edu; phone: 212-851-5462; or Isabelle Leclerq, isabelle.leclercq@uclouvain.be; phone 32-2764-5273

† These authors contributed equally.

Hepatocellular carcinoma (HCC) is the third leading cause of cancer mortality world-wide. Despite its nomenclature, the cellular origin of HCC remains elusive with hepatocytes and progenitor cells representing sources for newly generated hepatocytes in chronic liver injury and subsequently developing HCC. Determining the cellular source for HCC has high relevance for primary and secondary prevention strategies, as HCCs with progenitor signature carry a worse prognosis. Here, we employed complementary cell fate tracing approaches to label progenitor cells and hepatocytes in murine hepatocarcinogenesis. Tumors arose from hepatocytes but not progenitor cells in genetic, genotoxic and dietary HCC models. Almost all A6-, AFP- and cytokeratin 19-positive cells within tumors but not in the surrounding liver were derived from hepatocytes. In summary, our findings suggest that hepatocytes are the main source for HCC in mice, and that progenitor signature does not reflect progenitor origin but rather de-differentiation of hepatocyte-derived tumor cells.

INTRODUCTION

Hepatocellular carcinoma (HCC) is the third leading cause of cancer mortality world-wide with approximately 700,000 new cases diagnosed every year (1, 2). HCC typically develops in patients with chronic liver disease. Among these, viral hepatitis, non-alcoholic fatty liver disease and alcoholic liver disease are the leading causes for HCC (2). Chronic liver injury, triggering permanent <u>hepatocellular damage,</u> hepatocyte regeneration and inflammation, is thought to be the unifying principle that promotes carcinogenesis in these pathophysiologically distinct diseases. In the developing liver, bipotent hepatoblasts differentiate into hepatocytes and cholangiocytes and function as a main cellular source for both lineages (3). However, in the adult liver cell turnover is minimal, and bipotent progenitors are typically absent (3). As hepatocytes themselves are endowed with an almost infinite capacity to regenerate (4), regeneration following most types of injury or following partial hepatectomy is achieved from the hepatocyte pool without major contribution of progenitor cells (3, 5). However, when liver injury is chronic and when the ability of mature hepatocytes to proliferate is blocked, <u>a reserve cell compartment – often termed oval cells or liver progenitor cells (LPC) – expands in patients and in experimental injury models, and may contribute to the formation of hepatocytes (3, 4, 6-10). However, several recent fate tracing studies have challenged a major role for LPC in the formation of hepatocytes showing either no or only very little contribution to the hepatocyte pool (5, 11-15). On the other hand, the LPC/biliary compartment is capable to generate functional hepatocytes in zebrafish (16), indicating that the contribution of LPC may be model-, disease- or species-specific. Moreover, other studies support that hepatic stellate cells (HSCs) may function as multi-potent progenitor cells that generate functional hepatocytes and cholangiocytes (17). Thus,</u>

3

three different cellular sources, hepatocytes, LPC and HSCs, may in theory function as progenitor cells and cellular source for newly generated hepatocytes.

Despite its nomenclature, the cellular origin of HCC remains elusive. Of note, the expansion of LPC has most consistently been noted after treatment with hepatic carcinogens (18, 19), which has led to the suggestion that HCC may be derived from LPC (18, 20, 21). Moreover, the expression of progenitor markers and accumulation of LPC is commonly observed in rodent models as well as in human HCC (22, 23). Therefore, the reemergence of LPC in the chronically injured liver may link regeneration to hepatocarcinogenesis. Moreover, as HCC with a progenitor signature is clinically more aggressive, it has been suggested that the progenitor origin of HCC determines tumor biology and negatively affects outcome (23). Importantly, both LPC and hepatocytes have the capacity to generate tumors *in vivo* when transduced with H-Ras and SV40LT (24). However, the relative contribution of these two cell types to cancer formation in the context of chronic hepatocellular injury *in vivo* remains unknown. The high degree of plasticity in the liver is further highlighted by recent studies showing that cholangiocarcinoma can not only be derived from cholangiocytes (25) but also from hepatocytes (26, 27). Based on these findings in cholangiocarcinoma, it is conceivable that there are also multiple cellular sources for HCC. Using complementary strategies to label LPC, hepatocytes and HSCs, we demonstrate that hepatocytes but neither LPC nor HSCs function as cellular source for HCC. Moreover, LPC found in HCC were derived from hepatocytes, suggesting that hepatocyte-derived HCC may de-differentiate into an LPC-like immature phenotype.

RESULTS

HCC does not originate from liver progenitor cells.

To test the hypothesis that HCC is derived from the LPC compartment we used tamoxifen-inducible osteopontin-(OPN)-iCreER^{T2} x ROSA26R^{YFP} mice (OPN-Cre mice) to label progenitor and biliary cells. Tamoxifen injection in the post-natal period leads to recombination of the ROSA26R^{YFP} locus and to permanent expression of yellow fluorescent protein (YFP) in OPN-expressing cells. As reported elsewhere (12), upon tamoxifen injection, YFP expression is restricted to LPC and cholangiocytes and does not occur in hepatocytes, stellate, or Kupffer cells (Suppl.Fig.1). Using this system, between 69 and 82% of the progenitor and biliary compartment and their progeny were permanently tagged with YFP in this study (Fig.1C,H, Suppl.Fig.1A) and thus, development of YFP^{+}-HCC would indicate a progenitor/biliary origin.

First, HCCs were induced by chronic administration of diethylnitrosamine (DEN) resulting in HCC development in the setting of chronic injury, inflammation and fibrosis (28). Tamoxifen was injected at postpartum (pp) d21 (n=44) followed after a 4 week wash-out period by repeated DEN administration. At time of sacrifice, macroscopic tumors were observed in all livers (Fig.1A and Table 1), they were well delineated, and exhibited enlargement of the hepatocyte plates, high proliferative index, disruption of the reticulin network, absence of portal tracts and focal expression of α-fetoprotein (AFP) and OPN (Fig.1B-D). Altogether, 250 tumors were histologically evaluated by an experimental pathologist (C.S.) and diagnosed as HCC. YFP immunostaining was performed to determine the cell source of HCC. In all of 250 tumors, YFP expression was missing (Table 1) and only seen in CK-19+ and OPN+ bile

duct cells and ductular reaction (DR) that surrounds the tumors (Fig. 1C,D). In a second model, HCCs were induced by a single DEN injection to 15-day-old (d15) OPN-Cre mice. Tamoxifen was injected before (pp_d9-10; n=16) or after (pp_d21-22; n=25) DEN. The efficiency and specificity of the lineage tracing was equivalent (≈70%) and independent of the time of tamoxifen administration, and macroscopic tumors developed (Suppl.Fig.2A,B) in 50 and 70% of the mice within 18 and 9 months, respectively (Table 1), consistent with the notion that tamoxifen treatment, in particular when given immediately before tumor induction, delays or inhibits tumor development (29). 240 tumors induced by this method were diagnosed as HCC. YFP expression was absent in all HCC (Table 1), while bile ducts and the DR found surrounding the tumors were YFP-positive (Suppl.Fig.2C,D). These findings were further confirmed in OPN-CreERT2 mice treated with the combination DEN and CCl₄, which mimics hepatocarcinogenesis in the setting of liver fibrosis (30). In this model, HCCs also displayed typical features of HCC, including loss of collagen IV staining, high proliferation and expression of progenitor genes *AFP*, *Prom1*, and *H19* (Fig.1F,I). Again, none of the tumors were labeled with YFP whereas bile duct in non-tumor liver were YFP-positive (Fig.1F-H, Table 1). In a second model of LPC labeling, induced by the combination of tamoxifen-inducible K19-CreERT (31) and Cre reporter ZsGreen, none of the arising DEN+CCl₄-induced HCCs was derived from K19-CreERT-labeled LPC (Suppl.Fig.3, Table 1). In summary, the absence of LPC-labeled tumors confirms that in multiple genotoxic DEN-induced hepatocarcinogenesis models and in different Cre-transgenic mice for LPC labeling, HCCs do not arise from progenitor or biliary cells.

Genotoxic HCC originates from hepatocytes.

As we found no evidence for the LPC compartment serving as the cellular source of HCC, we

next investigated the alternative hypothesis that hepatocytes constitute the cellular source for HCC. To selectively label and trace hepatocytes during hepatocarcinogenesis, we employed an adeno-associated virus serotype 8, expressing Cre recombinase under the control of the hepatocyte-specific thyroxin-binding globulin promoter (AAV8-TBG-Cre) in combination with ROSA26$^{loxP-mTom-stop-loxP-\underline{m}GFP}$ (mTom/mGFP) or ROSA26$^{loxP-stop-loxP-ZsGreen1}$ (ZsGreen) Cre reporter mice. In ZsGreen Cre reporter mice, this approach labeled > 96% of hepatocytes, without labeling any other hepatic compartment including F4/80-positive Kupffer cells, the cytokeratin-positive biliary and LPC compartments, desmin-positive HSCs or endomucin-positive endothelial cells, as determined by immunohistochemistry and confocal imaging (Suppl.Fig.4A,C-G). This analysis was further confirmed by qPCR of FACS-sorted cells that expressed the green fluorescent Cre reporter ZsGreen and showed at least the same level of Alb and Ttr expression as primary hepatocytes, but virtually no expression of cholangiocyte markers *Krt7* and *Krt19*, HSC markers *Des* and *Lrat*, endothelial cell markers *Pecam* (CD31) and *vWF*, and macrophage markers *Emr1* (F4/80) and *Cd68* (Suppl.Fig.4B). Together, these data confirm efficient and highly specific labeling of hepatocytes by AAV8-TBG-Cre similar to previous studies (32, 33). Following AAV8-TBG-Cre infection at pp d12, we employed either single agent DEN (data not shown), or the combination of DEN+CCl$_4$ to trigger hepatocarcinogenesis. These well-established protocols resulted in the development of well-delinated tumors in 100% of mice (Fig.2A). Although the average hepatocyte labeling rate in the mTom-mGFP reporter mice was slightly below 96%, we observed an average rate of 99.7% macroscopically and microscopically mGFP-positive tumors (n=10 mice, 185 out of 186 tumors), i.e. hepatocyte-derived tumors, in DEN+CCl$_4$-treated mice (Fig.2A-D, Table 2). Because hepatocyte labeling did not reach 100% and because we never observed any tumor

arising from the LPC compartment by our complementary LPC labeling approaches, we consider it most likely that the single GFP-negative tumor arose from unlabeled hepatocytes rather than from the LPC compartment. Although tumors were macroscopically entirely green, microscopic analysis revealed the presence of unrecombined non-hepatocyte-derived Tomato-positive cells that consisted predominantly of CD31-positive endothelial cells and F4/80-positive macrophages, confirming hepatocyte-specific labeling by our approach also within tumors (Suppl.Fig.5). Tumors were clearly defined as HCCs by pathological examination, loss of the normal hepatic reticulin and collagen IV staining pattern, increased expression of the proliferation marker Ki67, altered expression pattern of Gp73, loss of β-catenin, upregulation of glutamine synthetase (Fig.2E). Histological analysis revealed a wide range of growth patterns including trabecular, steatotic, solid and cytoplasmatic inclusions (data not shown). Accordingly, tumors were diverse when analyzed by array comparative genomic hybridization (aCGH), demonstrating chromosomal aberrations in each investigated mouse, with a wide range of genomic alterations rather than a specific pattern (Fig.2F). Of note, comparison of genomic alteration in DEN+CCl$_4$-induced HCC to a well-characterized set of human cryptogenic HCC (34) demonstrated gains and losses of loci in various chromosomal regions congruent with genomic alterations in human HCC (Fig.2G), further confirming the relevance of the herewith employed model. Moreover, tumors expressed high levels of *Gpc3*, *Golm1*, *mKi67*, *Tff3* and *Tspan8* mRNA (Fig.2H). Importantly, every single DEN+CCl$_4$-induced tumor that we examined contained at least one magnitude higher expression levels of progenitor markers *Afp* and *H19*, and almost all also contained much higher levels of *Prom1* (Fig.2I). These data clearly exclude the possibility that hepatocyte origin in the DEN+CCl$_4$ model is due to the lack of progenitor signature in these tumors. To

8

additionally address the possibility that LPC origin may only be revealed in models in which HCC arises in the setting of higher progenitor cell presence and turnover, we employed the combination of DEN with either CDE diet or DDC diet (11, 12). Although the labeling of hepatocytes was less efficient in these experiments than in the above DEN+CCl$_4$ experiments, 98.3% of DEN+CDE-induced tumors and 95.6% of DEN+DDC-induced tumors being macroscopically and microscopically GFP-positive (Suppl.Fig.6A-D). When only mice with at least 90% hepatocytes labeling were included in the analysis, 100% of tumors were GFP-positive (data not shown), again suggesting that the few GFP-negative tumors in DEN+CDE and DEN+DDC experiments were a result of incomplete hepatocyte labeling rather than being LPC-derived. Similar to the DEN+CCl$_4$ model, DEN+CDE- and DEN+DDC-induced tumors showed high expression of HCC markers and progenitor markers (Suppl.Fig.6E-F, Table 2).

HCC originates from hepatocytes in non-genotoxic HCC models

To exclude that our observations on hepatocyte origin are specific to the employed models or caused by preferential metabolism of carcinogens in hepatocytes, we additionally tested cellular origin in DEN-free HCC models. For this purpose, we first investigated Mdr2^{ko} mice which spontaneously develop inflammation, fibrosis and HCC, thus reproducing the sequence of events that lead to the majority of human HCCs (35). In the Mdr2^{ko} model, AAV8-TBG-Cre-mediated hepatocyte labeling via ZsGreen Cre reporter exceeded 96.8%, without labeling desmin-positive HSCs, F4/80-positive Kupffer cells, cytokeratin-positive cholangiocytes, or endomucin-positive endothelial cells (Suppl.Fig.7A). As this model not only lacks

confounding effects of hepatocellular DEN metabolism but also incorporates an abundance of LPC markers in the injured liver (Fig.3H), it provides an ideal setting to test in an unbiased manner from which cell population HCCs derive in the chronically injured, inflamed and fibrotic liver. All HCCs from Mdr2^{ko} mice (n=7 mice, 20 out of 20 tumors) arose from AAV8-TBG-Cre labeled hepatocytes with macroscopic and microscopic ZsGreen tumor fluorescence (Fig.3A-D, Table 2) and co-localization of ZsGreen with HNF4α within tumors (Fig.3E). Tumors from Mdr2^{ko} mice were typical HCCs with altered collagen IV expression, high expression of proliferation marker Ki-67, and upregulation of *Golm1*, *mKi67*, *Tff3* and *Tspn8* mRNA (Fig.3F-G), as determined by immunohistochemistry and qPCR. The few ZsGreen-negative cells within tumors were endomucin-positive endothelial cells, F4/80-positive Kupffer cells (Suppl.Fig.7B). To further confirm these findings in another non-genotoxic model, we determined whether hepatocyte-specific deletion of PTEN triggers HCC. PTEN is a tumor suppressor gene that shows reduced expression in about 50% of human HCC and inverse correlation with survival (36), and whose deletion by Albumin-Cre – which deletes in both the hepatocyte and LPC/biliary compartment (Suppl.Fig.8) - triggers HCC development in mice (37). To provide evidence for hepatocytes as the cellular source of HCC in a genetic model, we either deleted PTEN specifically in hepatocytes via AAV8-TBG-Cre or in the progenitor/biliary compartment via tamoxifen-inducible K19-Cre-ERT (31) AAV8-TBG-Cre-induced hepatocyte-specific deletion of PTEN resulted in the development of tumors with HCC features including increased glypican_3, Ki-67, keratin and pAkt expression (Suppl.Fig.9A-B, Table 2) and tumors were derived from hepatocytes as demonstrated by green fluorescence (Suppl.Fig.9C,D). By contrast, K19-driven PTEN deletion resulted in an expansion of the cytokeratin-positive biliary compartment but never

10

led to HCC development (Suppl.Fig.9D-E). These data again demonstrate that the LPC/biliary compartment is not endowed with the capacity to form HCCs in mice. Finally, we also subjected OPN-Cre mice to chronic treatment with CDE-deficient diet as a complementary LPC labeling approach. This model was accompanied by a florid DR. HCCs were less common than in other models but were YFP-negative and hence not of LPC origin (Suppl.Fig.9G-H, Table 1). Together, these data provide multiple lines of evidence that hepatocytes and not LPC are also the cellular source of HCC in non-genotoxic tumor models.

Hepatic stellate cells do not represent a cellular source for HCC.

As HSCs have been show to act as an alternative source of LPC and hepatocytes (17), we wanted to determine whether HSC-derived LPC or hepatocytes may be the source for HCC. For this purpose, HSCs were labeled by Lrat-Cre in combination with ZsGreen or TdTomato mice, a system that efficiently and selectively tags HSCs in the liver (38). In line with our previous studies in multiple injury models (38), we did not detect a significant number of HSC-derived hepatocytes in mice that underwent injury-driven hepatocarcinogenesis induced by DEN+CCl$_4$ (data not shown). Moreover, we did not find any tumors that were derived from Lrat-Cre-labeled cells (Fig.4A-C), with all fluorescent cells within tumors being desmin-positive (Fig.4D) and HNF4α- and cytokeratin-negative (Suppl.Fig.10A). Similar observations were made in the Mdr2^{ko} model, where no tumor cell was derived from Lrat-Cre-labeled HSCs (Fig.4E,F,H, Suppl.Fig.10B). In both models, tumors revealed typical HCC characteristics such as altered collagen IV and Gp73 expression patterns and increased Ki-67 staining (Fig.4C,G). While most tumors contained moderate numbers of Lrat-Cre-labeled cells, some tumors in both the DEN+CCl$_4$ and Mdr2^{ko} models displayed stronger accumulation of Lrat-Cre-labeled desmin-positive HSCs (Suppl.Fig.10C,D). However, even

in the few tumors that showed strong Cre reporter fluorescence, fluorescent cells co-localized with desmin without any overlap of Lrat-Cre-induced Cre reporter TdTomato with either HNF4α or cytokeratin (Suppl.Fig.10E,F). These findings are consistent with our data on the exclusive contribution of hepatocytes to HCC formation in the DEN+CCl$_4$ and the Mdr2^{ko} models, and further exclude that HSC-derived hepatocytes as cellular source of HCCs.

Progenitor cells within HCCs originate from hepatocytes.

Consistent with our data showing high mRNA expression of progenitor markers *AFP*, *Prom1* and *H19* in tumors (Fig.1I, Fig.2I, Suppl.Fig.6F), we observed abundant A6- and AFP-positive, and to a lesser extent cytokeratin 19 (K19)-positive cells within HCC nodules in all DEN-based models, (Fig.1C,G, Fig.5A-C,E,F, Suppl.Fig.2C-D, Suppl.Fig. 11, Suppl.Fig.12A-B, Suppl.Fig.13A-B). Instead of interpreting these markers as a sign of progenitor, we investigated the alternative hypothesis that AFP-, A6- and cytokeratin 19-positive cells within HCC may be hepatocyte-derived cells that underwent de-differentiation. Confocal microscopy demonstrated that in AAV8-TBG-Cre mice virtually all A6-positive cells within DEN+CCl$_4$-, DEN+DDC- and DEN+CDE-induced tumors also co-expressed mGFP (Fig.5A, Suppl.Fig. 11, Suppl.Fig.12B, Suppl.Fig.13B), thus demonstrating their hepatocyte origin. These data were confirmed by AFP and K19 staining, which showed that AFP-positive cells (Fig.5C, Suppl.Fig.11, Suppl.Fig.12A, Suppl.13A) and K19-positive cells (Fig.5B, Suppl.Fig.11) within tumors were mGFP-positive and therefore hepatocyte-derived. In contrast, there were almost no A6-positive cells that co-expressed mGFP outside of the tumors (Fig.5A,D, Suppl.Fig.11, Suppl.Fig.12B, Suppl.Fig.13B). Moreover, only a low amount of K19-positive cells outside the tumor areas were mGFP-positive (Fig.5B,D). Similar findings were made in the Mdr2^{ko} model, in which most K19-positive and A6-

positive cells within tumors but not in the surrounding liver were hepatocyte derived (Suppl.Fig.14A-B). Consistent with these findings, we observed in OPN-Cre mice that A6-positive cells within tumors were YFP-negative whereas the A6-positive ductular reaction surrounding tumors was YFP-positive (Fig.5E,H). K19 staining confirmed that YFP-positive cells outside the tumors expressed K19 while K19-positive cells within HCC were YFP-negative (Fig.5F,H, Suppl.Fig.2C-D). AFP positive cells were only found within the tumors and were YFP negative (Fig. G). Together, these data suggest that A6-, K19 and AFP-positive cells within tumors are hepatocyte-derived, but that most A6- and K19-positive cells outside the tumors (AFP-positive cells were extremely rare outside tumors – Fig.5D) were derived from LPC/biliary compartment.

DISCUSSION

Despite its nomenclature, the cellular source of HCC remains elusive. Hepatocytes are not only the target of oncogenic hepatotrophic viruses and most hepatotoxins, but also have a stem-cell like capacity for nearly infinite regeneration (39), making them a primary candidate for the cellular source of HCC. In addition, LPC/biliary compartment not only has the capacity to differentiate into hepatocytes (7, 10, 16) but LPC also commonly found in dyplastic lesions and HCCs (22, 23, 40), suggesting that this compartment could be an alternative source for subsets of HCCs, in particular those with LPC signature. In support of this, both populations have been demonstrated to have the ability to induce HCC when transduced with a combination of H-Ras and SV40LT (24). Despite their know capacity to differentiate into HCC after forced expression of oncogenes, the relative contribution of these cell types to HCC formation in endogenous HCC models that occur in the setting of chronic

injury and inflammation remains unknown. Our fate tracing data support the hypothesis that hepatocytes constitute the main cellular source of HCC in mice and that LPC do not function as a source of HCC in mice. Our analysis not only includes several models in which HCCs expressed an abundance of progenitor markers, but also carcinogen-free models, in which HCC formation can be assessed without the possibly confounding preferential metabolization of carcinogenes by hepatocytes. Consistent with our data that 99.4% and 100% of HCC in the DEN+CCl$_4$ and Mdr2^{ko} model, respectively, were hepatocyte-derived, we never observed HCCs developing from genetically-labeled LPC. Due to the early age at which mice were injected, our hepatocyte labeling did not reach the levels that were seen in adult mice in previous studies (11, 32). As we did not label all hepatocytes but nonetheless only observed a single GFP-negative tumor out of a total of 186 tumors and none in the Mdr2^{ko} model, we conclude that this tumor most likely arose from unlabeled hepatocytes. This is consistent with our finding that HCCs were never LPC-derived when we labeled the LPC/biliary compartment. Moreover, we did not find any evidence supporting HSC, a recently suggested alternative source for liver progenitors and hepatocytes (17), as cellular source of HCC. Our findings are consistent with recent studies showing either a dominant or even exclusive role of hepatocytes in hepatocyte repopulation, even in settings where LPC expand and were considered a key source of newly generated hepatocytes (11-15). Likewise, our finding that murine HCCs are not derived from HSCs is consistent with our previous finding that HSCs do not contribute to the hepatocyte or progenitor pool in multiple chronic injury models in mice (38). In agreement with the data presented here, a recent study using Hnf1a-CreERT labeling of the biliary/LPC compartment, found no contribution of LPC to HCC in DEN- or Mdr2^{ko}-induced HCC (41), which complements findings presented here. However, in contrast to our

study, the authors did not positively identify the cellular source for HCC.

Recent studies found that hepatocytes have a high degree of plasticity and de-differentiate into immature progenitors or biliary-type cells in response to specific signals (32, 33). These data are consistent with our finding that hepatocyte-derived tumor cells express progenitor markers, suggesting a similar ability of hepatocyte-derived tumor cells to de-differentiate into progenitor-like cells. It is likely that such a de-differentiation allows cells to adapt to specific challenges in the environment and presents an advantage for the tumor. Accordingly, tumors with progenitor signature have worse prognosis (23). Our study contains several limitations. Although we have confirmed hepatocyte-origin and excluded progenitor origin and HSC origin for a number of HCC models including various genotoxic and genetic models, we cannot fully exclude that progenitors have the ability to generate tumors in other settings. As a wide range of infectious, metabolic, genetic and toxic liver diseases can result in HCC development in patients, studies in additional hepatocarcinogenesis models – possibly employing humanized mice to mimick HCC arising in the setting of HBV- and HCV-induced hepatitis - are required to broaden the presented findings. Also, recent fate tracing studies in zebrafish have suggested that when hepatocyte proliferation is completely blocked – which so far has not been achieved in murine injury models – regeneration occurs to a significant degree from the biliary compartment (16). However, a "catastrophic" event with complete hepatocyte failure is characteristic for acute liver failure but not for HCC, where injury is typically mild and chronic, similar to the employed animal models. Despite strong evidence in murine models, our study has only model character for human hepatocarcinogenesis. Our study mimicked several key features that are characteristic for human hepatocarcinogenesis, such as chronic liver injury, fibrosis and alterations of PTEN expression, but cannot address

possible intrinsic differences between mouse and human hepatocytes or progenitor cells. As such, the contribution of ductular reaction to functional hepatocytes in humans remains a matter of debate (40), and it therefore cannot be excluded that ductular reaction is a cellular source of HCC in patients. Future studies need to address the cellular origin of human HCC, e.g by showing that human hepatocytes have the same plasticity as mouse hepatocytes and are able to de-differentiate into progenitor cells and/or the use of humanized mice for fate tracing.

MATERIALS AND METHODS

All animal experiments were performed with approval from the Université catholique de Louvain Animal Welfare Committee and the Columbia University IACUC in accordance with EU regulations and NIH guidelines for the care and use of laboratory animals, respectively.

Tracing of liver progenitor cells in hepatocarcinogenesis. To track the LPC and biliary cells, we used the previously reported OPN-iCreER^{T2};ROSA26R^{YFP} mice (12). The transgenic mice have a CD1-enriched background and males were used in all experiments. To achieve Cre-LoxP recombination, tamoxifen (Sigma, T5648, Diegem, Belgium) dissolved in corn oil at a concentration of 30 mg/ml was injected intraperitoneally (i.p.) at 100 mg/kg body weight (BW) at day 21 pp unless specified otherwise. In all experiments, transgenic mice without tamoxifen injection (n ≥5) were used in parallel as negative control for Cre recombination. Mice had free access to water and food at all times. To determine the contribution of LPC to HCC, tamoxifen i.p. at d21 pp was followed by weekly DEN i.p. (35 mg/kg BW) for 25 weeks starting at 6 weeks of age (n=44) (28). At the start of chronic DEN treatment and up to the end of the experiment, one group of mice was fed a standard rodent

16

chow (n=22) while another group (n=22) was placed on a high fat diet (HFD, 60% saturated fat, D12492 from Research Diets, USA). Because the effect of HFD was to hasten tumor development, and not the nature of the tumors, data are presented for the entire group. In a second model a single i.p. of DEN (6 mg/kg BW, Sigma-Aldrich, N0258, Diegem, Belgium) at d15 pp and tamoxifen i.p. either at d 9-10 pp (n=16) or d 21-22 pp (n=25) and were sacrificed at 18 or 9 months, respectively. In a third experiment, tamoxifen-injected mice (d9-10 pp) followed by a single i.p. of DEN (6 mg/kg BW- d15pp) and 20 weekly subsequent injections of CCl_4 (0.5 µl/g body weight). Mice were sacrificed 2 to 4 weeks after last CCl_4 dose (n=6). The DEN+CCl_4 model was additionally performed in K19-CreERT2 mice co-expressing either ZsGreen or TdTomato Cre reporter, receiving tamoxifen at pnd10, and DEN at pnd 15, followed by 25 CCl_4 injections. Other tamoxifen injected (pnd 21) OPN-Cre mice (n=12) were treated with choline-deficient, 0.15% ethionine-supplemented (CDE) diet for 50 weeks starting at 8 weeks of age. Mice were sacrificed at 58 weeks of age or earlier, when the general status of mice was altered (BW loss, decreased activity, or prostration). The DEN+CCl_4 model was additionally performed in K19-CreERT2 mice (n=4) co-expressing either ZsGreen or TdTomato Cre reporter, receiving tamoxifen (80 µg/g i.p.) at d10 pp, and DEN at d15 pp, followed by 25 CCl_4 injections.

Tracing of hepatoytes in hepatocarcinogenesis. To genetically label hepatocytes, lox-stop-lox mTom-mGFP Cre reporter mice (42) were infected with AAV8-TBG-Cre, resulting in mGFP expression in AAV8-TBG-Cre infected hepatocytes and their offspring. For this purpose, mice were injected with $1x10^{11}$ genome copies of AAV8-TBG-Cre (43) intravenously (i.v.) at d12 pp. To induce HCC, AAV8-TBG-Cre infected mice received a

single i.p. of DEN (25 mg/kg BW, Sigma-Aldrich) at d15 pp. Subsequently, hepatic carcinogenesis was promoted by chronic injury using three different models. Four weeks after receiving DEN, some mice were treated with a total of 15 injections of carbon tetrachloride (CCl_4, 0.5 µl/g i.p., dissolved in oil at ratio of 1:3, given once weekly, n=7) as described (30). For hepatocyte tracing in mice receiving DEN+CCl_4, only mice with at least 90% hepatocyte labeling in non-tumor sections were analyzed. Some mice were fed for 6 weeks with 0.1% 3,5-diethoxycarbonyl-1,4-dihydro-collidin (DDC)-containing diet (n=4) starting 4 weeks after receiving DEN. Some mice were fed for 6 weeks with choline-deficient, 0.15% ethionine-supplemented (CDE) diet starting 4 weeks after DEN injection (n=5).

Mdr2 knockout-mediated hepatocarcinogenesis. To genetically label hepatocytes in the Mdr2[ko] model, lox-stop-lox ZsGreen Cre reporter mice (44) were infected with AAV8-TBG-Cre, resulting in ZsGreen expression in AAV8-TBG-Cre infected hepatocytes and their offspring. Mdr2[ko] mice (FVB background) that had been bred with ZsGreen Cre reporter mice (C57Bl/6 background) and once backcrossed with Mdr2[ko] mice, were injected with $1x10^{11}$ genome copies of AAV8-TBG-Cre (43) intravenously (i.v.) at d14 pp. Mdr2[ko] mice received additionally up to 25 CCl_4 injections in order to accelerate hepatocarcinogenesis. Mice were sacrificed at the age of 12-14 months following HCC screening by ultrasound.

PTEN-mediated hepatocarcinogenesis studies. As a non-genotoxic model of HCC, PTEN[f/f] mice, some of which were additionally carrying the mTom/mGFP Cre reporter, were injected with AAV8-TBG-Cre ($1x10^{11}$ genome copies i.v.) at 7 weeks of age, resulting in hepatocyte-specific deletion of PTEN. To delete PTEN specifically in the progenitor/ductular compartment, Krt19-CreERT mice (31) were crossed with floxed PTEN mice, and injected with tamoxifen (100 µg/ i.p.) at 2 weeks of age.

18

LratCre-mediated HSC labeling. To determine whether HSCs might be a cellular source for HCC, LratCre mice co-expressing ZsGreen or TdTomato Cre reporters (44) were injected DEN (25 mg/kg BW, i.p) at d15 pp followed by 20 injections of CCl_4. Mice were sacrificed 2 weeks after the last CCl_4 injection. $Mdr2^{ko}$ mice co-expressing LratCre and ZsGreen or TdTomato served as second HCC model. Mice were sacrificed at the age of 12-14 months following HCC screening by ultrasound.

Immunohistochemical and immunofluorescent analysis. Following sacrifice, and rapid excision of the liver rapidly, tumor and non-tumor tissue were macroscopicall identified and either fixed in 4% formalin for histological examination, or snap frozen in liquid nitrogen for gene expression analysis.

For histological analysis, four μm formalin-fixed, paraffin-embedded liver sections and frozen liver sections were analyzed. For immunohistochemistry, slides were incubated for 1 hour at 37ºC with primary antibodies against YFP (Ab6673, Abcam), cytokeratin 19 (Developmental studies Hybridoma bank, University of Iowa), HNF4α (PP-H1415, R&D Systems or SC-6556, Santa Cruz Biotechnology), alpha feto protein (14550-1-AP, Proteintech), osteopontin (AF808, R&D Systems), alpha smooth muscle actin (Mybiosource San Diego, CA), Ki67 (Tec3, Dako), desmin (RB-9014-P, Lab Vision), pancytokeratin (Z0622, Dako), CD31 (14-0311-81, Ebioscience), progenitor marker A6 (45) (a gift from Dr. Valentina Factor) or F4/80 (MCA497A64, AbD serotec), collagen IV (CL50451 AP-1, Cedarlane), Ki67 (Rabbit monoclonal, ThermoScientific), Gp73 (sc-48001, Santa Cruz) or glutamine synthetase (ab16802, Abcam). Detection was either performed using fluorescent secondary antibodies with various fluorescent conjugates anti-rabbit (donkey anti-rabbit, A21207, chicken-anti-rat A21472 or chicken anti-goat A21468, all used at 1:200, all

Invitrogen), or by HRP-conjugated secondary antibodies (anti-rat Ig-HRP, E0468, anti-goat Ig-HRP P0449, anti-mouse Envision K4001 or anti-rabbit Envision K4003, used at 1:50-1:200, all DAKO), with subsequent diaminobenzidine (DAB) exposure and hematoxylin counterstaining. For DAB staining, serial sections were used. Fluorescent images were taken on a Nikon A1 confocal laser microscope (Nikon Instruments, Melville, NY, USA) using 20x standard lens or 40x and 60x oil-immersion lenses or an Axiovert 200 fluorescent microscope (Carl Zeiss, Munich, Germany). For some pictures and for quantification, four to six sections were merged. Non-fluorescent images were taken with a Zeiss microscope coupled to an AxioCam camera (MR3, Carl Zeiss, Munich, Germany). Omission of the first antibody with otherwise identical procedure or sample lacking specific protein expression served as negative control.

Quantification of hepatocyte and tumor labeling ratio. Labeling efficiency in the biliary/progenitor compartment was determined as previously reported [8] by quantification of K19$^+$/YFP$^+$ double positive cells relative to the total number of K19-positive cells in 25 random non-tumor fields of view per section per mouse, and expressed as percentage. Timing for tamoxifen injection (d9 to d21) or DEN treatment at d15 did not modify labeling efficiency. The percentage of A6$^+$/YFP$^+$ and AFP$^+$/YFP$^+$ double positive cells were quantified using the same methodology.

For macroscopic imaging and determination of the percentage of GFP-labeled tumors, livers were visualized under a Leica MZ 16F fluorescent dissecting microscope. The ratio between green tumors and all tumors per mouse was determined and expressed as a percentage. To quantify the GFP labeling for hepatocytes, frozen sections from non-tumor tissue were used.

Labeling efficiency was evaluated by quantification of GFP+ hepatocytes relative to the total number of GFP+ and mTomato+ hepatocytes. and expressed as a percentage.

The percentage of K19+/GFP+ double-positive cells was determined by quantification of K19+/GFP+ double-positive cells relative to total K19+ cell number in tumor and non-tumor areas in DEN+CCl$_4$, DEN+CDE, DEN+DDC treated mice groups. The percentage of A6+/GFP+ double-positive cells was determined by the same approach.

RNA isolation and qPCR. RNA was isolated from cells and liver tissue by column purification and on-column DNAse treatment. After reverse transcription, mRNA levels were determined by quantitative real-time PCR on an Applied Biosystem 7300 PCR cycler, using Applied Biosystems Taqman primers and probes for *Afp*, *Prom1, H19, mKi67*, *Golm1*, *Tspan8, Tff3 and Gpc3*. All qPCRs were quantified using relative standard curves, and normalized to expression of 18s. mRNA levels in OPN-Cre samples were determined using SybrGreen and results expressed as fold induction relative to control untreated liver using the ΔΔCt method.

Determination of hepatocyte and non-parenchymal cell markers in AAV8-TBG-Cre-labeled liver cells. To determine which hepatic cell types were labeled by AAV8-TBG-Cre, ZsGreen Cre reporter mice were infected with AAV8-TBG-Cre. One week later, mice were sacrificed. Following perfusion with collagenase, green-fluorescence cells were sorted from the entire liver cell suspensions by FACS. After RNA isolation and reverse transcription, qPCR was employed to measure hepatocyte markers (*Alb*, *Ttr*), cholangiocyte markers (*Krt7*, *Krt19*), HSC markers (*Des*, *Lrat*), endothelial cell makers (*Pecam*, *vWf*), and macrophage markers (*Emr1*, *Cd68*). To determine the percent of these markers in the isolated green-

21

fluorescent cell fraction, cDNA from pure reference populations of primary cholangiocytes, HSCs, endothelial cells and hepatic macrophages (38) were used.

Comparative genomic hybridization and syntenic analysis. Custom-designed 8x60k arrays (AMADID 41078 were used for array CGH (Agilent, Bloebingen, Germany). 19 different formalin-fixed and paraffin embedded HCC nodules and two unaffected liver tissues were microdissected and genomic DNA was extracted using DNAeasy FFPE kit (QIAGEN; Hildesheim, Germany), as described (46). 125 ng gDNA from test and control DNA were labeled with Cy3-dUTP and Cy5-dUTP, respectively, using CGH labeling protocol of Enzo Life Sciences (Enzo, Loerrach, Germany). Purification of labeled nucleotides, hybridization, scanning and data extraction were performed according to manufacturer's instructions and as described (47). 50% of estimated proportion of tumor cells - based on H&E microscopic assessments - were used for the CGHcall function (46, 47). Human syntenic regions were queried using an in-house compiled R-Function (REF21) and Biomart database (www.biomart.com). Ward's method and Euclidean distance were employed to hierarchically cluster and visualize the copy number profiles, using again the in-house written R function. The aCGH set described in (34) was downloaded from GEO (http://www.ncbi.nlm.nih.gov/geo/query/acc.cgi?acc=GSE8351) and analyzed as described (47) .

Statistical evaluation. Statistical analysis was performed using Prism (GraphPad, San Diego, CA). Differences between two groups were calculated using Student's t-test (paired t-test) or Mann-Whitney U-test. Significance of differences between multiple groups was determined

by one-way ANOVA, followed by Dunnett's or Dunns post-hoc test. All data are expressed as means ± standard deviation.

REFERENCES

1.   Parkin DM, Bray F, Ferlay J, and Pisani P. Estimating the World Cancer Burden: Globocan 2000. *Int J Cancer.* 2001;94(2):153-6.
2.   Forner A, Llovet JM, and Bruix J. Hepatocellular Carcinoma. *Lancet.* 2012;379(9822):1245-55.
3.   Miyajima A, Tanaka M, and Itoh T. Stem/Progenitor Cells in Liver Development, Homeostasis, Regeneration, and Reprogramming. *Cell Stem Cell.* 2014;14(5):561-74.
4.   Zaret KS, and Grompe M. Generation and Regeneration of Cells of the Liver and Pancreas. *Science.* 2008;322(5907):1490-4.
5.   Friedman JR, and Kaestner KH. On the Origin of the Liver. *J Clin Invest.* 2011;121(12):4630-3.
6.   Wilson JW, and Leduc EH. Role of Cholangioles in Restoration of the Liver of the Mouse after Dietary Injury. *J Pathol Bacteriol.* 1958;76(2):441-9.
7.   Wang X, Foster M, Al-Dhalimy M, Lagasse E, Finegold M, and Grompe M. The Origin and Liver Repopulating Capacity of Murine Oval Cells. *Proc Natl Acad Sci U S A.* 2003;100 Suppl 1(11881-8.
8.   Boulter L, Lu WY, and Forbes SJ. Differentiation of Progenitors in the Liver: A Matter of Local Choice. *J Clin Invest.* 2013;123(5):1867-73.
9.   Duncan AW, Dorrell C, and Grompe M. Stem Cells and Liver Regeneration. *Gastroenterology.* 2009;137(2):466-81.
10.   Huch M, Gehart H, van Boxtel R, Hamer K, Blokzijl F, Verstegen MM, Ellis E, van Wenum M, Fuchs SA, de Ligt J, et al. Long-Term Culture of Genome-Stable Bipotent Stem Cells from Adult Human Liver. *Cell.* 2015;160(1-2):299-312.
11.   Malato Y, Naqvi S, Schurmann N, Ng R, Wang B, Zape J, Kay MA, Grimm D, and Willenbring H. Fate Tracing of Mature Hepatocytes in Mouse Liver Homeostasis and Regeneration. *J Clin Invest.* 2011;121(12):4850-60.
12.   Espanol-Suner R, Carpentier R, Van Hul N, Legry V, Achouri Y, Cordi S, Jacquemin P, Lemaigre F, and Leclercq IA. Liver Progenitor Cells Yield Functional Hepatocytes in Response to Chronic Liver Injury in Mice. *Gastroenterology.* 2012;143(6):1564-75 e7.
13.   Yanger K, Knigin D, Zong Y, Maggs L, Gu G, Akiyama H, Pikarsky E, and Stanger BZ. Adult Hepatocytes Are Generated by Self-Duplication Rather Than Stem Cell Differentiation. *Cell Stem Cell.* 2014;15(3):340-9.
14.   Tarlow BD, Pelz C, Naugler WE, Wakefield L, Wilson EM, Finegold MJ, and Grompe M. Bipotential Adult Liver Progenitors Are Derived from Chronically Injured Mature Hepatocytes. *Cell Stem Cell.* 2014;15(5):605-18.
15.   Schaub JR, Malato Y, Gormond C, and Willenbring H. Evidence against a Stem Cell Origin of New Hepatocytes in a Common Mouse Model of Chronic Liver Injury. *Cell Rep.* 2014;8(4):933-9.
16.   He J, Lu H, Zou Q, and Luo L. Regeneration of Liver after Extreme Hepatocyte Loss Occurs Mainly Via Biliary Transdifferentiation in Zebrafish. *Gastroenterology.* 2014;146(3):789-800 e8.
17.   Kordes C, Sawitza I, Gotze S, Herebian D, and Haussinger D. Hepatic Stellate Cells Contribute to Progenitor Cells and Liver Regeneration. *J Clin Invest.* 2014;124(12):5503-15.
18.   Sell S. Is There a Liver Stem Cell? *Cancer Res.* 1990;50(13):3811-5.

19. Sigal SH, Brill S, Fiorino AS, and Reid LM. The Liver as a Stem Cell and Lineage System. *Am J Physiol.* 1992;263(2 Pt 1):G139-48.

20. Roskams T. Liver Stem Cells and Their Implication in Hepatocellular and Cholangiocarcinoma. *Oncogene.* 2006;25(27):3818-22.

21. Andersen JB, Loi R, Perra A, Factor VM, Ledda-Columbano GM, Columbano A, and Thorgeirsson SS. Progenitor-Derived Hepatocellular Carcinoma Model in the Rat. *Hepatology.* 2010;51(4):1401-9.

22. Roskams TA, Libbrecht L, and Desmet VJ. Progenitor Cells in Diseased Human Liver. *Semin Liver Dis.* 2003;23(4):385-96.

23. Lee JS, Heo J, Libbrecht L, Chu IS, Kaposi-Novak P, Calvisi DF, Mikaelyan A, Roberts LR, Demetris AJ, Sun Z, et al. A Novel Prognostic Subtype of Human Hepatocellular Carcinoma Derived from Hepatic Progenitor Cells. *Nat Med.* 2006;12(4):410-6.

24. Holczbauer A, Factor VM, Andersen JB, Marquardt JU, Kleiner DE, Raggi C, Kitade M, Seo D, Akita H, Durkin ME, et al. Modeling Pathogenesis of Primary Liver Cancer in Lineage-Specific Mouse Cell Types. *Gastroenterology.* 2013;145(1):221-31.

25. Guest RV, Boulter L, Kendall TJ, Minnis-Lyons SE, Walker R, Wigmore SJ, Sansom OJ, and Forbes SJ. Cell Lineage Tracing Reveals a Biliary Origin of Intrahepatic Cholangiocarcinoma. *Cancer Res.* 2014;74(4):1005-10.

26. Fan B, Malato Y, Calvisi DF, Naqvi S, Razumilava N, Ribback S, Gores GJ, Dombrowski F, Evert M, Chen X, et al. Cholangiocarcinomas Can Originate from Hepatocytes in Mice. *J Clin Invest.* 2012;122(8):2911-5.

27. Sekiya S, and Suzuki A. Intrahepatic Cholangiocarcinoma Can Arise from Notch-Mediated Conversion of Hepatocytes. *J Clin Invest.* 2012;122(11):3914-8.

28. Heindryckx F, Mertens K, Charette N, Vandeghinste B, Casteleyn C, Van Steenkiste C, Slaets D, Libbrecht L, Staelens S, Starkel P, et al. Kinetics of Angiogenic Changes in a New Mouse Model for Hepatocellular Carcinoma. *Mol Cancer.* 2010;9(219.

29. Veronesi U, Boyle P, Goldhirsch A, Orecchia R, and Viale G. Breast Cancer. *Lancet.* 2005;365(9472):1727-41.

30. Dapito DH, Mencin A, Gwak GY, Pradere JP, Jang MK, Mederacke I, Caviglia JM, Khiabanian H, Adeyemi A, Bataller R, et al. Promotion of Hepatocellular Carcinoma by the Intestinal Microbiota and Tlr4. *Cancer Cell.* 2012;21(4):504-16.

31. Means AL, Xu Y, Zhao A, Ray KC, and Gu G. A Ck19(Creert) Knockin Mouse Line Allows for Conditional DNA Recombination in Epithelial Cells in Multiple Endodermal Organs. *Genesis.* 2008;46(6):318-23.

32. Yanger K, Zong Y, Maggs LR, Shapira SN, Maddipati R, Aiello NM, Thung SN, Wells RG, Greenbaum LE, and Stanger BZ. Robust Cellular Reprogramming Occurs Spontaneously During Liver Regeneration. *Genes Dev.* 2013;27(7):719-24.

33. Yimlamai D, Christodoulou C, Galli GG, Yanger K, Pepe-Mooney B, Gurung B, Shrestha K, Cahan P, Stanger BZ, and Camargo FD. Hippo Pathway Activity Influences Liver Cell Fate. *Cell.* 2014;157(6):1324-38.

34. Schlaeger C, Longerich T, Schiller C, Bewerunge P, Mehrabi A, Toedt G, Kleeff J, Ehemann V, Eils R, Lichter P, et al. Etiology-Dependent Molecular Mechanisms in Human Hepatocarcinogenesis. *Hepatology.* 2008;47(2):511-20.

35. Trauner M, Fickert P, and Wagner M. Mdr3 (Abcb4) Defects: A Paradigm for the Genetics of Adult Cholestatic Syndromes. *Semin Liver Dis.* 2007;27(1):77-98.

36. Hu TH, Huang CC, Lin PR, Chang HW, Ger LP, Lin YW, Changchien CS, Lee CM, and Tai MH. Expression and Prognostic Role of Tumor Suppressor Gene Pten/Mmac1/Tep1 in Hepatocellular Carcinoma. *Cancer.* 2003;97(8):1929-40.

37. Horie Y, Suzuki A, Kataoka E, Sasaki T, Hamada K, Sasaki J, Mizuno K, Hasegawa G, Kishimoto H, Iizuka M, et al. Hepatocyte-Specific Pten Deficiency Results in Steatohepatitis and Hepatocellular Carcinomas. *J Clin Invest.* 2004;113(12):1774-83.

38. Mederacke I, Hsu CC, Troeger JS, Huebener P, Mu X, Dapito DH, Pradere JP, and Schwabe RF. Fate Tracing Reveals Hepatic Stellate Cells as Dominant Contributors to Liver Fibrosis Independent of Its Aetiology. *Nat Commun.* 2013;4(2823.

39. Overturf K, al-Dhalimy M, Ou CN, Finegold M, and Grompe M. Serial Transplantation Reveals the Stem-Cell-Like Regenerative Potential of Adult Mouse Hepatocytes. *Am J Pathol.* 1997;151(5):1273-80.

40. Fausto N. Liver Regeneration and Repair: Hepatocytes, Progenitor Cells, and Stem Cells. *Hepatology.* 2004;39(6):1477-87.

41. Jors S, Jeliazkova P, Ringelhan M, Thalhammer J, Durl S, Ferrer J, Sander M, Heikenwalder M, Schmid RM, Siveke JT, et al. Lineage Fate of Ductular Reactions in Liver Injury and Carcinogenesis. *J Clin Invest.* 2015.

42. Muzumdar MD, Tasic B, Miyamichi K, Li L, and Luo L. A Global Double-Fluorescent Cre Reporter Mouse. *Genesis.* 2007;45(9):593-605.

43. Miller RA, Chu Q, Le Lay J, Scherer PE, Ahima RS, Kaestner KH, Foretz M, Viollet B, and Birnbaum MJ. Adiponectin Suppresses Gluconeogenic Gene Expression in Mouse Hepatocytes Independent of Lkb1-Ampk Signaling. *J Clin Invest.* 2011;121(6):2518-28.

44. Madisen L, Zwingman TA, Sunkin SM, Oh SW, Zariwala HA, Gu H, Ng LL, Palmiter RD, Hawrylycz MJ, Jones AR, et al. A Robust and High-Throughput Cre Reporting and Characterization System for the Whole Mouse Brain. *Nat Neurosci.* 2010;13(1):133-40.

45. Engelhardt NV, Factor VM, Medvinsky AL, Baranov VN, Lazareva MN, and Poltoranina VS. Common Antigen of Oval and Biliary Epithelial Cells (A6) Is a Differentiation Marker of Epithelial and Erythroid Cell Lineages in Early Development of the Mouse. *Differentiation.* 1993;55(1):19-26.

46. Vucur M, Reisinger F, Gautheron J, Janssen J, Roderburg C, Cardenas DV, Kreggenwinkel K, Koppe C, Hammerich L, Hakem R, et al. Rip3 Inhibits Inflammatory Hepatocarcinogenesis but Promotes Cholestasis by Controlling Caspase-8- and Jnk-Dependent Compensatory Cell Proliferation. *Cell Rep.* 2013;4(4):776-90.

47. Haybaeck J, Zeller N, Wolf MJ, Weber A, Wagner U, Kurrer MO, Bremer J, Iezzi G, Graf R, Clavien PA, et al. A Lymphotoxin-Driven Pathway to Hepatocellular Carcinoma. *Cancer Cell.* 2009;16(4):295-308.
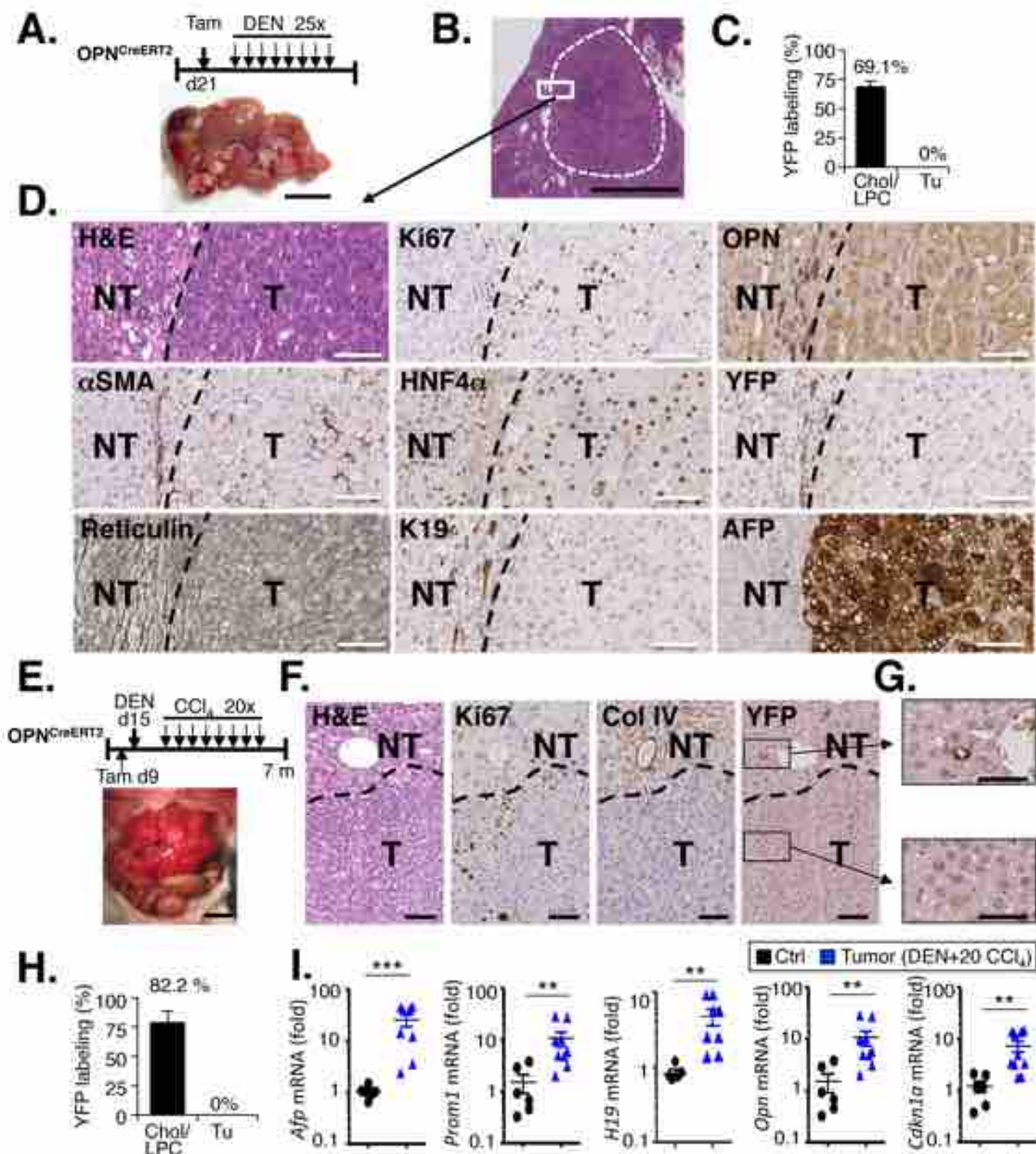
Figure 1. Hepatocellular carcinoma does not derive from the biliary/LPC compartment. A-D. Tamoxifen-treated OPN-CreERT2 mice expressing YFP Cre reporter subjected to 25 DEN injections (n=33) developped HCC (A-B). While the K9+ biliary /LPC compartment was tagged efficiently by YFP, no HCC was YFP positive (C). HCC were delineated by α-SMA positive border and infiltrated by myofibroblasts; HCC displayed a disrupted reticulin meshwork, high Ki67 expression, focally expressed OPN and AFP and were surrounded by a patchy K19-positive and YFP-positive ductular reaction (D). E-I. Tamoxifen-treated OPN-CreERT2 mice were treated with DEN followed by 20 CCl₄ injections (n=6). Representative macroscopic (E) and histological images (F) showing typical HCC features such as high Ki67 and disruption of the collagen IV meshwork. The cholangiocyte/LPC compartment but no HCCs were YFP positive (G,H). HCC and progenitor markers determined by qPCR (I). Scale Bar A,B,E: 1 cm; D,F: 100 μm; G: 50 μm. ** p<0.01 and ***p<0.001
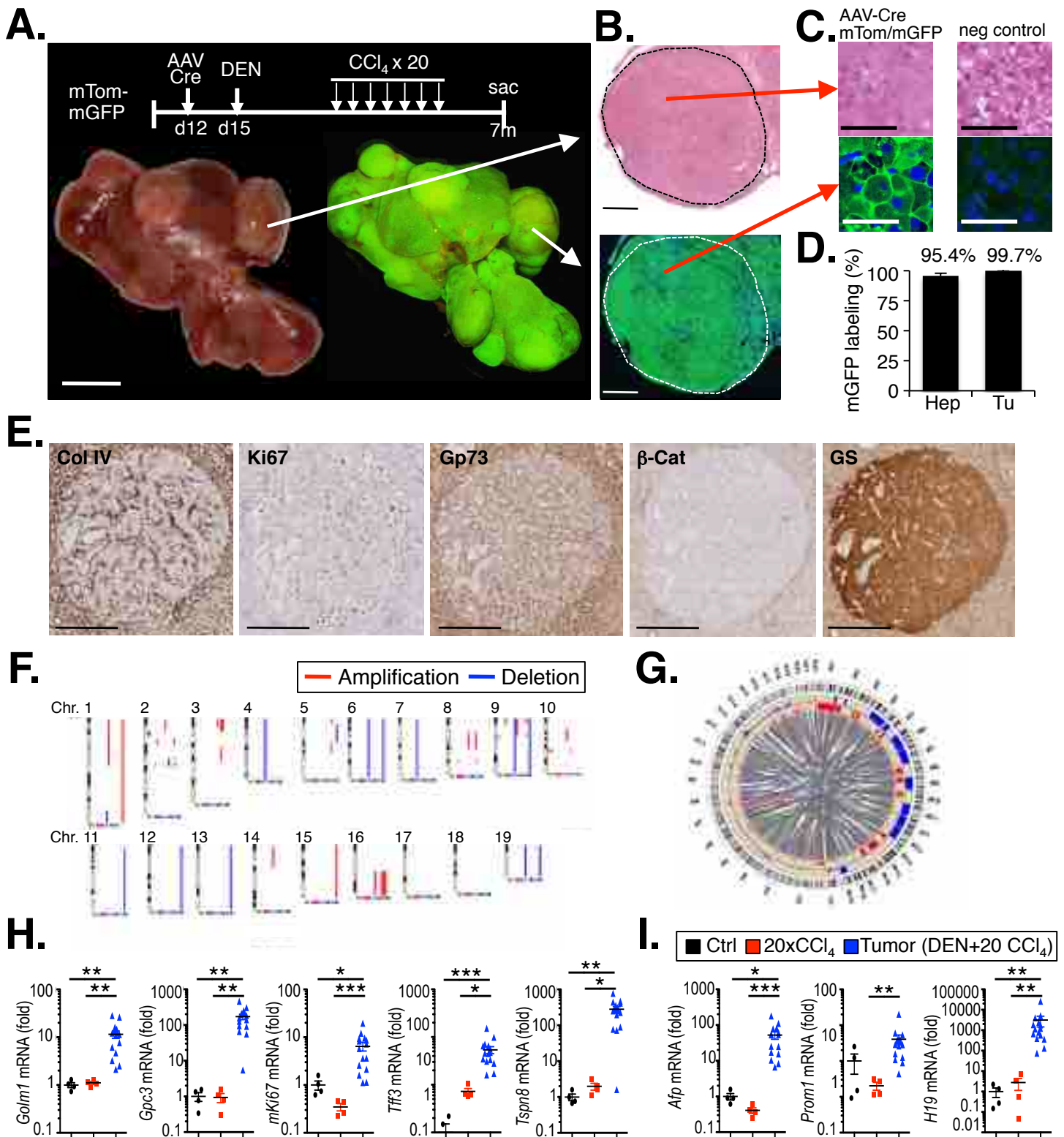
Figure 2. Genotoxic HCC derives from hepatocytes. mTom-mGFP Cre reporter mice (n=10) were infected with AAV8-TBG-Cre to selectively label hepatocytes, followed by treatment with DEN and 15 CCl$_4$ injections for HCC induction. **A-C.** Representative photographs and fluorescent images of livers from DEN +CCl$_4$ treated mice (A) and H&E- and GFP-stained liver sections at low (B) and high (C) magnification, including a mTom-mGFP-negative control. **D.** Quantification of GFP-labeled hepatocytes and tumors (average of all mice). **E**. Typical HCC features were confirmed by collagen IV staining, increased Ki67 and glutamine synthetase and altered Gp73 and β-catenin staining. **F-G.** Karyoplot (F) of comparative genomic hybridization array from 19 tumors (from different 8 different mice). Long (q) arm is shown, dark band representing G-C rich domain. Synteny analysis (G) reveals that loci with chromosomal losses (blue) or amplifications (red) in the DEN+CCL$_4$ model are also found in human HCCs. **H-I.** HCC markers (H) and progenitor markers (I) were determined by qPCR. Scale bars: A: 1 cm; B: 1 mm; C: 50 μm E: 300 μm
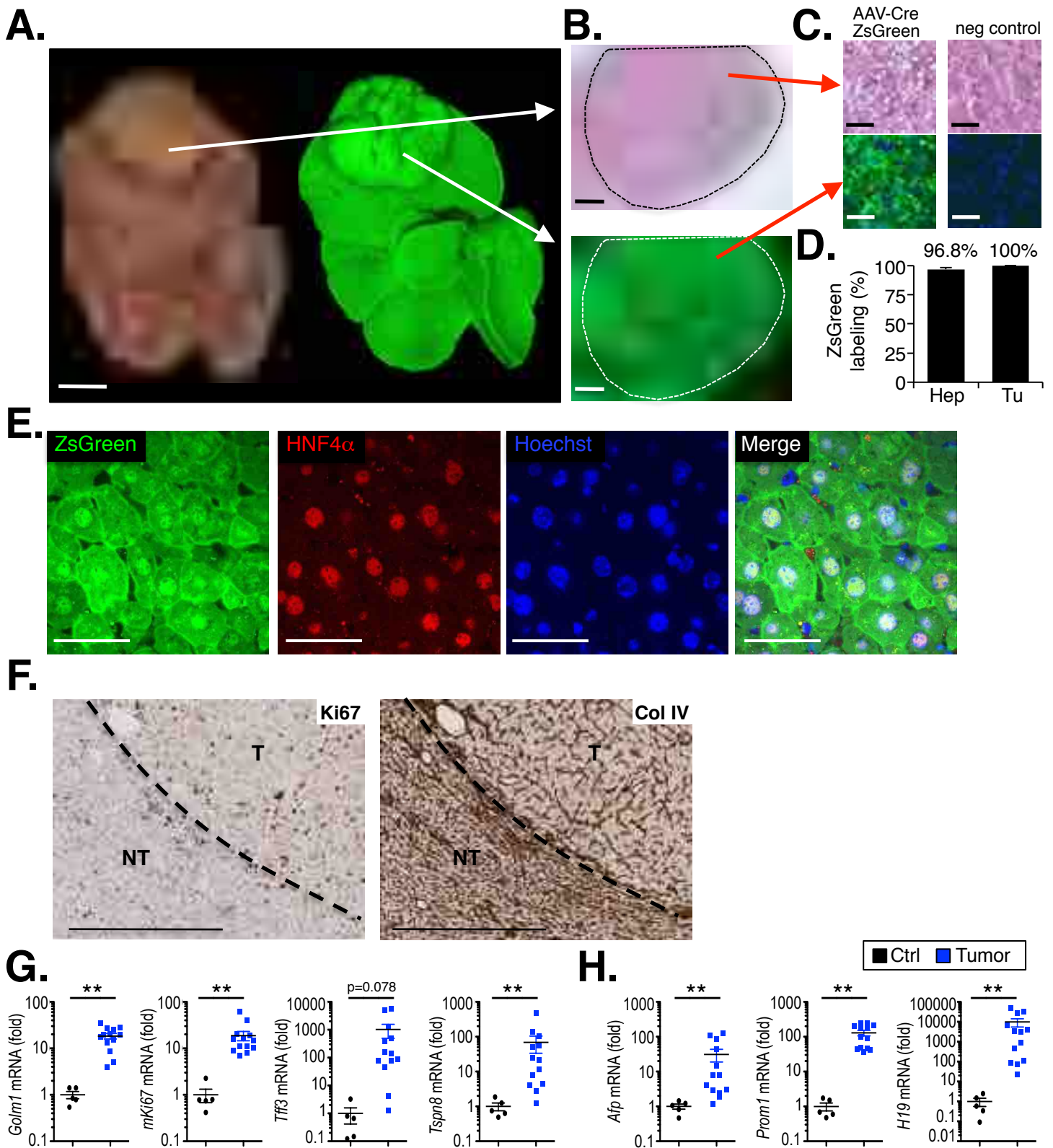
Figure 3. HCCs derive from hepatocytes in the Mdr2^{ko} HCC model. ZsGreen Cre reporter mice (n=8) were infected with AAV8-TBG-Cre to selectively label hepatocytes, and sacrificed at the age of 12-14 months. **A-C.** Representative photographs and fluorescent images of whole livers from Mdr2^{ko} mice (A) as well as low power H&E- and DAP-stained frozen liver sections at low (B) and high (C) power including a ZsGreen-negative control. **D.** Quantification of GFP-labeled hepatocytes and tumors (average of all mice). **E.** Co-staining demonstrated that HNF4α-positive tumor cells were ZsGreen positive. **F.** Typical HCC features were confirmed by increased Ki67 expression and altered collagen IV staining. **G-H.** HCC markers (F) and progenitor markers (G) were determined by qPCR. Scale bar A:1 cm; B: 300 μm; C,E 50 μm; F: 500 μm. ** p<0.01.
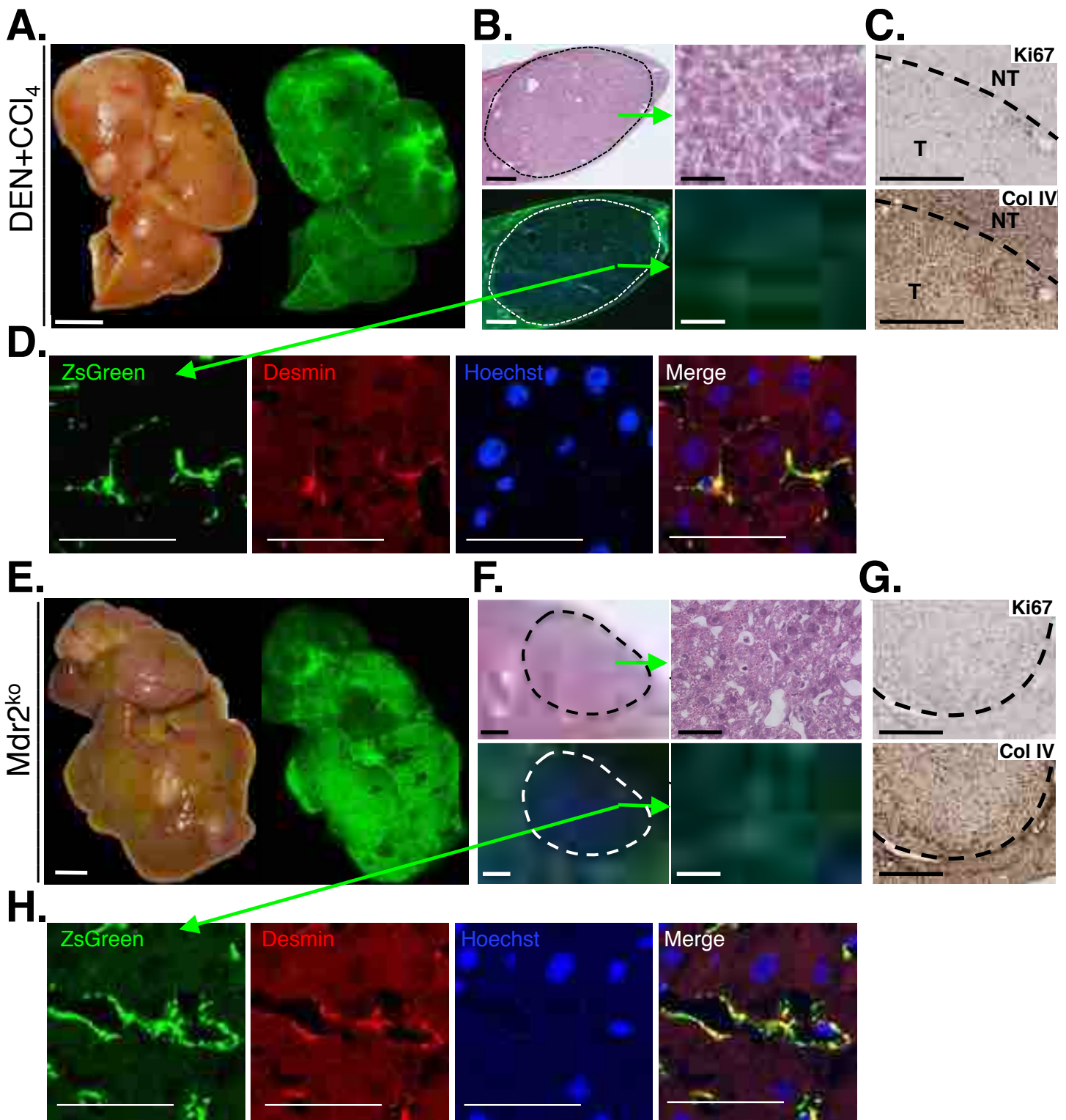
Figure 4. HCCs are not derived from hepatic stellate cells. A-D. LratCre transgenic mice expressing ZsGreen Cre reporter (n=4) were treated with DEN and 15 CCl_4 injections for HCC induction. Representative photographs and fluorescent images of livers from DEN+CCl_4 treated mice (A) as well as low and high power H&E- and Hoechst-stained frozen liver sections at low and high magnification show green fluorescent HSCs but no green fluorescent tumor cells derived from HSCs (B). Typical HCC features were confirmed by collagen IV staining and increased Ki67 expression (C). ZsGreen-positive cells colocalized with HSC marker desmin (D). **E-H.** Mdr2[ko] mice expressing LratCre and the Zs1Green Cre reporter (n=8) were sacrificed at the age of 12 months. Representative photographs and fluorescent images of whole livers (E) as well as low and high power H&E- and Hoechst-stained frozen liver sections at low and high magnification show green fluorescent HSCs but no green fluorescent tumor cells derived from HSCs (F). Typical HCC features were confirmed by increased Ki67 expression and altered collagen IV staining (G). ZsGreen-positive cells colocalized with HSC marker desmin (H). Scale bar: A and E: 5 mm; B (left panel) and F (left panel): 500 μm; B (right panel) and F (right panel): 50 μm; C and G 500 μm; D and H 50 μm.
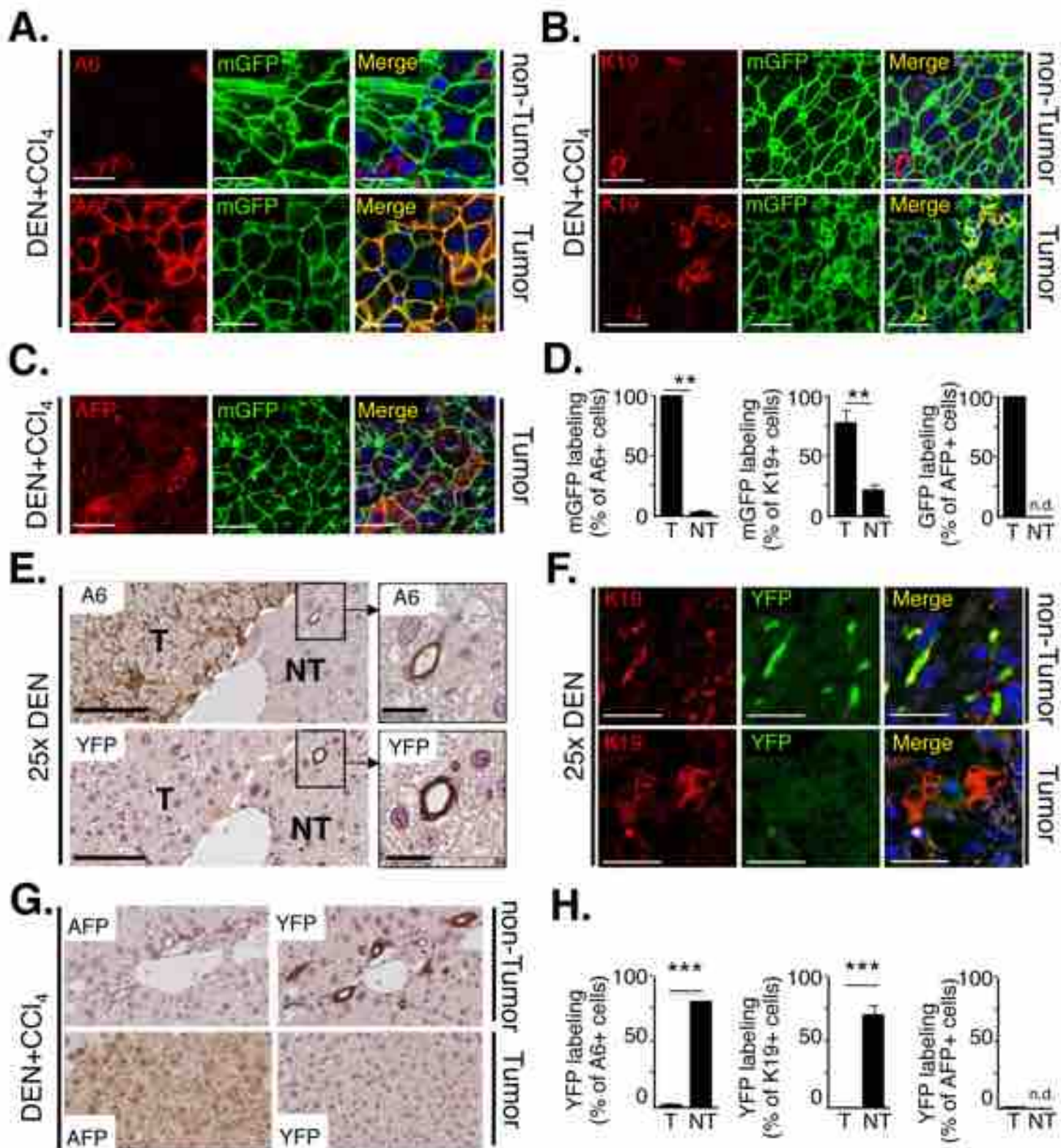
Figure 5. A6-, K19- and AFP-positive liver progenitors within HCCs are derived from hepatocytes.
A-D. To determine the cellular origin of liver progenitor cells within HCCs, colocalization of progenitor markers A6 (A), K19 (B) and AFP (C) with mGFP was determined by confocal microcopy in tumor and non-tumor areas of mTom-mGFP mice whose hepatocytes had been labeled via AAV8-TBG-Cre and that were subsequently treated with DEN and CCl_4. Quantification of mGFP of A6+, K19+ and AFP+ cells in tumor (T) and non-tumor (NT) areas (D). **E-H.** Colocalization of progenitor markers A6 (E, serial sections), K19 (F, fluorescence) and AFP (G, serial sections) with YFP in tumor (T) and non-tumor (NT) areas of OPN-CreERT2 mice treated with 25xDEN injections or DEN+CCl_4. Quantification of YFP with A6+, K19+ or AFP+ cells (H) in tumor or non-tumor areas. **p<0.01,***p<0.001; n.d.=non-detectable. Scale bars A-C, E, F: 50 μm.

Table 1: LPC tracking in HCC models.

Mouse	HCC Induction	Liver analyzed (n)	Livers with HCC (%)	Number of HCC analyzed per liver (min-max)	Total number of HCC analyzed	% of HCC traced as of LPC origin	% of K19+ HCC (number of pos HCCs/ total number of total analyzed tumors)	% of A6+ HCC (number of pos HCCs and number of total analyzed tumors)
OPN-CreERT2	TAM d21 / DEN 25X	33	100%	1->25	>250	0	2% (5 /250 analyzed)	14.7% (17/115 analyzed)
OPN-CreERT2	DEN d15/TAM d21-22	25	68%	1-20	>150	0	0% (0 / 150 analyzed)	Not determined
OPN-CreERT2	DEN d15/TAM d9-10	16	50%	4-20	>90	0	0% (0 / 90 analyzed)	26% (13/50 analyzed
OPN-CreERT2	TAM d9-10/DEN d15/CCl_4 20x	6	100%	1-15	30	0	0% (0/30 analyzed)	66.6% (20/30 analyzed)
OPN-CreERT2	CDE diet > 1yr	9	30%	1-2	4	0	0	Not determined
K19-CreERT	TAM d10 DEN+CCl_4	4	100%	25-69	187	0	10.7% (13/121 analyzed)	33.1% (40/121 analyzed)
PTEN$^{f/f}$ - K19-CreERT	PTEN deletion in LPC (TAM d21)	4	0%	n/a	n/a	n/a	n/a	n/a

Table 2: Hepatocyte tracking in HCC models.

Mouse	HCC Induction	Liver analyzed (n)	Livers with HCC (%)	Number of HCC analyzed per liver (min–max)	Total number of HCC analyzed	% of HCC traced as of hepatocyte origin	% of K9+ HCC (number of pos HCCs and number of total analyzed tumors)	% of A6+ HCC (number of pos HCCs and number of total analyzed tumors)
lox-stop-lox mTom-mGFP Cre reporter mice + AAV8-TBG-Cre	DEN+CCl$_4$	10	100%	1-35	186	99.5% (185/186)	17.1% (19/111 analyzed)	36.9% (41/111 analyzed)
lox-stop-lox mTom-mGFP Cre reporter mice + AAV8-TBG-Cre	DEN+CDE	4	100%	19-41	118	98.3% (116/118)	14.5% (12/83 analyzed)	56.6% (47/83 analyzed)
lox-stop-lox mTom-mGFP Cre reporter mice + AAV8-TBG-Cre	DEN+DDC	3	100%	5-22	46	95.7% (44/46)	11.4% (4/35 analyzed)	40.0% (14/35 analyzed)
Mdr2^{ko} - ZsGreen Cre reporter mice + AAV8-TBG-Cre	Mdr2^{ko}	7	100%	1-6	20	100% (13-133)	38.4% (5/13 analyzed)	76.9% (10/13 analyzed)
PTEN$^{f/f}$ - mTom/mGFP Cre reporter mice	PTEN deletion (AAV8-TBG-Cre)	8	100%	2-4	12	100% (123/123)	not determined	not determined
PTEN$^{f/f}$ - mTom/mGFP Cre reporter mice	PTEN deletion (AAV8-TBG-Cre)	4	100%	15-44	123	100% (123/123)	not determined	not determined